Draft version November 30, 2021
Typeset using LaTeX **RNAAS** style in AASTeX631

Measuring Stellar Heartbeats: an Asteroseismic Analysis of KIC7431665

Grace E. Chiodo[1]

[1] *Villanova University, 800 Lancaster Avenue, Villanova, PA 19085, USA*

ABSTRACT

Heartbeat binaries represent a class of red giant stars that receive particular attention in astronomy for their solar-like oscillations. Asteroseismology takes advantage of stellar pulsations to probe the interiors of stars that would otherwise be unobservable. In this study, we conduct a detailed asteroseismic analysis of the **heartbeat binary** KIC7431665 from *Kepler* data to determine the fundamental parameters of the system. **The analysis converts the light curve into a power spectrum to identify the oscillation modes present and the frequencies associated with them. We find $\nu_{max} = 54.5 \pm 0.4$ μHz for the frequency at maximum power and $\Delta\nu = 5.47 \pm 0.01$ μHz for the large separation frequency.** Applying scaling relations to the frequency results for KIC7431665 yields the following stellar parameters: R = 9.58 $\pm$ 0.08 $R_\odot$, M = 1.43 $\pm$ 0.03 $M_\odot$, L = 36.2 $\pm$ 0.59 $L_\odot$, and log(g) = 2.63 $\pm$ 0.001 dex **for the stellar radius, mass, luminosity, and logarithm of the surface gravity, respectively. This study effectively updates the stellar parameters for KIC7431665 and provides preliminary steps in understanding its internal structure.**

1. INTRODUCTION

One success of NASA's *Kepler* Space Telescope (2009-2018) stems from the unexpected discovery of a new class of stellar binaries: a heartbeat binary. **Kumar et al. (1995) first theorized the effects of a highly eccentric binary system on the tidal excitation of the modes in the system. The *Kepler* mission confirmed his theory with observations of tidally-induced flux variations (Welsh et al. 2011). Light curves of heartbeat binaries depict flux modulations at periastron, known as the heartbeat event, corresponding to heating and strong gravitational distortion that temporarily stretch the star (Themeßl et al. 2018).** The discovery presents an opportunity for asteroseismic analyses on the structure of the new stellar class by studying the high-resolution observations in the *Kepler* field of view. A heartbeat star can be further classified based on the type of stars within the system (Beck et al. 2014). Heartbeat red giant binaries, for example, consist of a red giant and a binary companion (Bedding & Kjeldsen 2010). A red giant star contains a helium core with a hydrogen-burning shell surrounded by a convective envelope (LeBlanc 2010). An asteroseismic analyses of solar-like oscillations in the exterior layers of the red giant determines the fundamental parameters and the details of the internal structure of the heartbeat binary.

A unique feature of heartbeat red giants is that they exhibit two forms of variability: solar-like oscillations and binary interactions. As with the oscillations observed for the Sun, a convective envelope drives the solar-like oscillations of heartbeat red giants (Themeßl et al. 2018). The convective movement of plasma transports energy and dampens oscillations (Bedding & Kjeldsen 2003). **These oscillations get amplified in heartbeat stars due to the highly eccentric orbit and the heartbeat event.** Another distinguishing feature of heartbeat red giants is that an oscillation pattern extends across all inclinations in the light curve, rather than the narrow range of the eclipse (Beck et al. 2014). This allows more extensive measurements of binary characteristics compared to other types of binary stars.

The mode of each oscillation depends on the restoring force. Pressure (p) modes cause radial motion due to the pressure gradient, while gravity (g) modes cause transverse motion due to buoyancy (Bedding et al. 2011). **Each mode is more sensitive in a particular region inside the star.** In the case of red giants, p modes dominate the solar-like oscillations in the convective envelope, while g modes have the largest amplitudes in the core. **(Beck et al. 2014)**. The non-radial modes of oscillation continuously work to restore a star to its equilibrium configuration. The trajectory of a wave inside a star deviates from the radial symmetry found in an approximately spherical object. The

Table 1. The table contains the values from literature for KIC7431665. Reference 1 corresponds to the study conducted by Beck et al. (2014), and reference 2 contains data from *Gaia EDR3* Brown et al. (2021).

Parameter	Value	Reference
Radius	$9.4 \pm 0.1\ R_{\odot}$	1
Mass	$1.39 \pm 0.05\ M_{\odot}$	1
Log(g)	2.62	1
$T_{\rm eff}$	4580 K	1
Distance	$939.952^{+13.873}_{-13.474}$ pc	2
Mean g magnitude	10.94894	2

oscillating behavior generates repeated variations in the radiation observed from variable stars as the star continuously attempts to return to its equilibrium form (LeBlanc 2010). These variations receive detailed study in the field of asteroseismology because they reflect the internal processes of a star that would otherwise be unobservable.

The fundamental properties obtained in asteroseismic analyses derive from various scaling relations. The scaling relations for stellar mass and radius depend on the pulsation frequencies and largest separation frequency from the power spectrum. **The relations also depend on the effective temperature because convection only becomes an oscillation mechanism of a star at certain temperatures (radiation occurs in zones of insufficient temperatures) (Bedding & Kjeldsen 2003).** Huber et al. (2012) presents a comparison of the fundamental properties determined with asteroseismic scaling relations to those determined from near-model-independent methods. The comparison shows good agreement between the two methods, which confirms the accuracy of fundamental parameters obtained with asteroseismic techniques. The scaling relations remain the preliminary method of extracting parameters from stellar pulsations (e.g. Hon et al. (2020); De Moura et al. (2020); Zhang et al. (2020)). Moreover, the scaling relations provide a reliable method of determining fundamental properties of heartbeat red giants and other stars that exhibit solar-like oscillations.

The preliminary studies of the fundamental properties of heartbeat red giants involved statistical analyses of large data sets. Beck et al. (2014) conducted an asteroseismic study of 18 eccentric binaries with data from the *Kepler Space Telescope* (Borucki et al. 2010). **The sample included the heartbeat binary KIC7431665, a red giant branch star with a binary companion (Frasca et al. 2016). KIC7431665 resides at a right ascension of 287.3750 degrees and a declination of 43.0094 degrees (Brown et al. 2021).** The results from the study yield the following estimates for KIC7431665: a mass of $1.39 \pm 0.05\ M_{\odot}$ and a radius of $9.4 \pm 0.1\ R_{\odot}$. Table 1 details the estimated parameters from the Beck et al. (2014) study. These parameters effectively reflect the red giant alone rather than an average of the binary companions due to the large size of the red giant. The red giant dominates the observational properties of a heartbeat binary unless the companion star is of high density, such as a white dwarf. The high resolution of the observations from the *Kepler* mission allows for more extensive asteroseismic analyses of red giant binaries (Cherinka et al. 2019).

The following study presents a detailed asteroseismic analysis of the heartbeat red giant KIC7431665 using the most recent *Kepler* data **to update the stellar parameters and create an Échelle diagram for investigating the oscillation modes.** Section 2 details the observations performed from the *Kepler* mission. Section 3 outlines the analysis of this data with the methods of obtaining stellar parameters from the light curve and power spectrum. Section 4 discusses the significance of the study and the next step for future ones. In Section 5, we reflect on the results of the study and the importance of obtaining stellar parameters.

2. OBSERVATIONS

The observations for KIC7431665 span Q0-Q17 of long cadence observations from the *Kepler Space Telescope* from 2009 to 2013 (Borucki et al. 2010). The *Kepler Input Catalog* (KIC) contains one ephemeris for this data with a period of 281.4 ± 0.0028 days **(Brown et al. 2011).** The long cadence has 6.02 second exposures and 0.52 second readout times. This yields 29.4 minute observations by integrations over 270 exposures (Gilliland et al. 2010). We generate normalized light curves of the *Kepler* photometric observations from the photometric flux data already compiled in the catalog **(see *Fig. 1*).** The effective temperature applied for **scaling relations in this study (see *Equations 3-5*)** is 4580 K from the results of Beck et al. (2014) analyzing *Kepler* data (Q0-Q14).

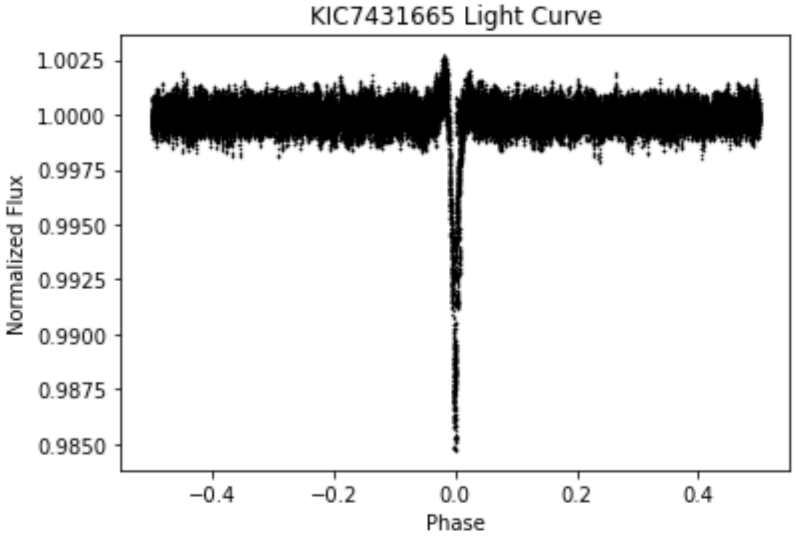

Figure 1. The figure displays the light curve for KIC7431665 phased with a period of 281.4 days from normalizing the *Kepler* flux data. The drop in flux represents the heartbeat event that causes gravitational distortions of the primary on its approach at periastron.

3. SEISMIC ANALYSIS

3.1. Stellar Parameters

The *Kepler* observations provide the photometric data necessary for generating light curves of the normalized flux and the corresponding **Barycentric Kepler Julian Dates (BKJD)**. We combine the individual light curves from Q0-Q17 to produce a light curve spanning across all observation windows **(see Fig. 2)**. The light curve contains large variations due to the highly eccentric orbit of the binary companions. **In addition to noise, these variations introduce flux variations unrelated to the internal oscillations of the star. We remove these eclipses, setting all normalized flux values above 1.0015 or below 0.9985 equal to the zero value, which is a normalized flux of one in this case. Removing the extreme values in the light curve reduces the flux variations unrelated to the solar-like oscillations.**

The light curve must be converted to a power spectrum to locate the region of excess power, a frequency range that displays power spikes of equal spacing. We investigate the region of excess power because it contains the signatures of the solar-like oscillation modes. We use the LIGHTKURVE python package to continue the seismic analysis of the solar-like oscillations (Lightkurve Collaboration et al. 2018). The LIGHTKURVE software includes the Lomb-Scargle method, **developed by (Lomb 1976) and (Scargle 1982)**, as a built-in function to construct a periodogram from the light curve data. **The Lomb-Scargle method calculates the amplitude spectrum of a time series of sampled data with gaps and unequal spacing (Seilmayer et al. 2020).** *Figure 3* displays the power density spectrum for KIC7431665. We normalize the power and zoom in on the region of excess power (30-80 μHz). A Gaussian fit approximates the mode envelope containing the oscillation modes (see *Fig. 3*). The mode envelope contains the frequency information necessary to calculate stellar parameters from scaling relations. The spikes in power in this region correspond to modes of oscillation. Equal frequency intervals separate modes of the same radial order (ie. radial or dipole modes).

The initial power spectral density data contains noise from the convective background and tidally-induced flux modulations from the heartbeat event. We remove this noise by flattening the power spectrum with a triangular filter (filter width = 7 days) via box smoothing. **Box smoothing removes noise by determining the average of all points inside a region of the specified filter width then replacing those values with the average and moving the filter along the curve. Applying the box filter to the curve twice produces the triangular filter, or the convolution of two rectangles (Guzik et al. 2016). *Figure 3* displays the smoothed power spectrum used for the remainder of the analysis.**

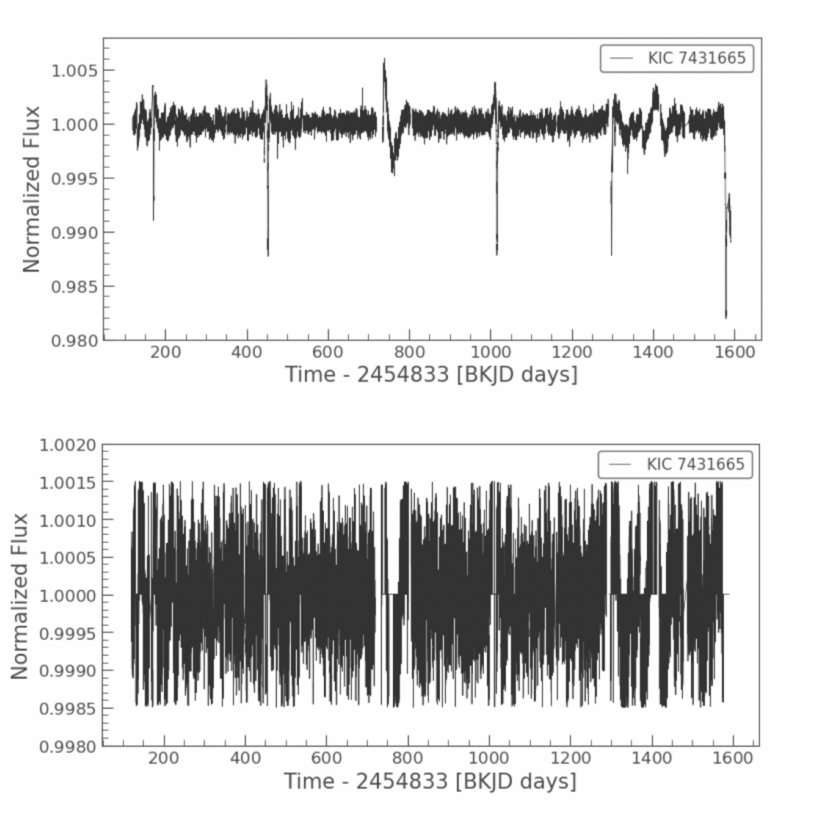

Figure 2. The upper panel displays the light curve data for KIC7431665. The light curve combines Q0-Q17 of *Kepler* observations. The large drops in the normalized flux correspond to eclipses of the binary companions. **The lower panel removes the extreme flux variation to focus on the solar-like oscillations happening within in the red giant.**

We then obtain the peak frequency of the excess of oscillation power, ν_{max}, by running a two-dimensional autocorrelation function on the smoothed power spectrum via Lightkurve, which adapts the methods of Viani et al. (2019). The two-dimensional autocorrelation function for red giant branch stars in the LIGHTKURVE package shifts windows of 25 μHz **(compared to 250 μHz for main sequence stars)** along the data in steps of 1 μHz to evaluate the correlation of the data with itself. The package then calculates the mean collapsed correlation of the two-dimensional autocorrelation function results to determine the frequency associated with the highest autocorrelation:

$$\mathrm{MCC} = \frac{\sum(|C|) - 1}{\mathrm{nlags}} \tag{1}$$

where *nlags* represents the number of times the autocorrelation was found for each frequency, and *C* defines the autocorrelation power at the central frequency for each iteration. The frequency associated with the peak of a one-dimensional Gaussian fit to the mean collapsed correlation yields the value of ν_{max}. We find that the *Kepler* data for KIC7431665 has $\nu_{max} = 54.50 \pm 0.4$ μHz. The uncertainty range results from a boostrapping analysis of the *Lightcurve* methods (discussed shortly).

The result for ν_{max} becomes an essential parameter in the calculation for $\Delta\nu$, **the large frequency separation between consecutive radial modes (Beck et al. 2014). The Lightkurve package determines $\Delta\nu$ by evaluating one full-width-half-max window on either side of ν_{max} in the power spectrum then adapting the methods of Mosser & Appourchaux (2009).** This ensures that the window includes all visible oscillation modes. **The method from Mosser & Appourchaux (2009) then estimates an empirical value for $\Delta\nu$ with the following calculation:**

$$\Delta\nu = 0.294 \times (\nu_{max})^{0.772} \tag{2}$$

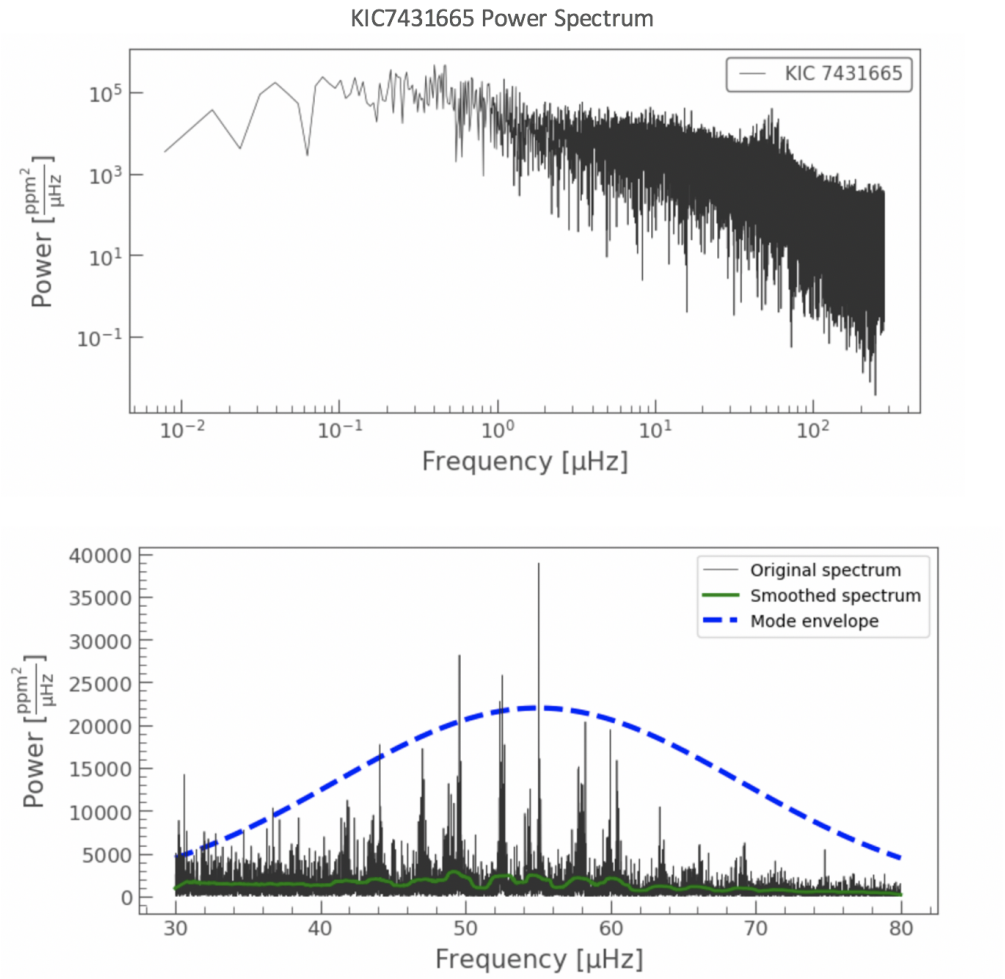

Figure 3. The figure contains the power spectral density of the *Kepler* light curve of KIC7431665. The upper panel includes the entire power spectrum, and the lower panel focuses on the region of power excess. The region of excess power has a Gaussian fit for the mode envelope and a smoothed spectrum (filter width = 7 days) overlayed on the data.

The spike in the autocorrelation function that most closely matches the empirical estimate for $\Delta\nu$ becomes the true value of $\Delta\nu$ for the study. We find $\Delta\nu = 5.47 \pm 0.01$ μHz for KIC7431665.

The uncertainty ranges for the stellar parameters result from the standard error and error propagation analyses. We determine the standard error from a bootstrapping resampling **process (Efron 1979).** We consider the light curve data to be the entire population set and then generate a random sample from that data. A function constructs the power spectrum for that sample and calculates ν_{max} and $\Delta\nu$ for the sample using the same LIGHTKURVE code from the initial analysis presented above. **We then resample the population with 1,000 iterations. Each iteration calculates the new ν_{max} and $\Delta\nu$ values, and we determine the average and standard deviation of those results.** We calculate the uncertainty ranges for ν_{max} and $\Delta\nu$ by dividing the final standard deviations by the square root of number of iterations.

We then calculate the mass, radius, and luminosity for KIC7431665 with the following scaling relations:

$$\frac{R_*}{R_\odot} = \frac{\nu_{max}}{\nu_{max}^\odot} * \left(\frac{\Delta\nu}{\Delta\nu_\odot}\right)^{-2} * \sqrt{\frac{T_{eff}}{T_{eff}^\odot}} \tag{3}$$

$$\frac{M_*}{M_\odot} = \left(\frac{R_*}{R_\odot}\right)^3 * \left(\frac{\Delta\nu}{\Delta\nu_\odot}\right)^2 \tag{4}$$

$$\frac{L_*}{L_\odot} = \left(\frac{\nu_{max}}{\nu_\odot}\right)^2 * \left(\frac{\Delta\nu}{\Delta\nu_\odot}\right)^{-4} * \left(\frac{T_{eff}}{T_{eff}^\odot}\right)^5 \tag{5}$$

where $R_\odot$, $M_\odot$, $L_\odot$, and $T_{eff}^\odot$ represent the solar radius, mass, luminosity, and effective temperature, respectively. We adopt solar values of ν_{max} and $\Delta\nu$ from Huber et al. (2011) and the solar effective temperature from Prša et al. (2016). The scaling relations yield the following parameters: R = 9.58 ± 0.08 $R_\odot$, M = 1.43 ± 0.03 $M_\odot$, and L = 36.2 ± 0.59 $L_\odot$. The bootstrapping analysis provided uncertainty ranges for the frequency values ν_{max} and $\Delta\nu$ which we extend to the uncertainties of the stellar parameters due to their dependence of the scaling relations on frequency. The error propagation calculations for the scaling relations take the square root of the sum of the squares of the propagation of errors $(\sigma_i \frac{\partial f}{\partial x_i})$ for each variable from this study that contains error (ie. ν_{max} and $\Delta\nu$).

A relation for surface gravity stems from the asteroseismic scaling relations as well:

$$g_* = g_\odot + \left(\frac{\nu_{max}}{\nu_{max}^\odot}\right) * \left(\frac{T_{eff}}{T_{eff}^\odot}\right)^{0.5} \tag{6}$$

where $g_\odot$ represents the solar surface gravity, and g_* represents the surface gravity of the target star. We again adopt the solar asteroseismic parameters from Huber et al. (2011) and the solar effective temperature from Prša et al. (2016) then apply the error propagation technique for the uncertainty range. **We find log(g) = 2.63** ±0.001 **dex.**

3.2. Échelle Diagram

The LIGHTKURVE package generates an Échelle diagram of the power spectrum. **An Échelle diagram slices the in lengths of $\Delta\nu$ then stacks these slices on top of one another.** This creates vertical ridges that correspond to modes of equal radial degree (Bedding & Kjeldsen 2010). In the Échelle created in this study, we see clear ridges for the oscillation modes (see *Fig. 3*) with oscillation modes of l=1, 2, and 0 corresponding to the ridges from left to right. **We determined the modes of oscillation for KIC7431665 visible in the Échelle diagram via the analysis of Carrier & Eggenberger (2006).**

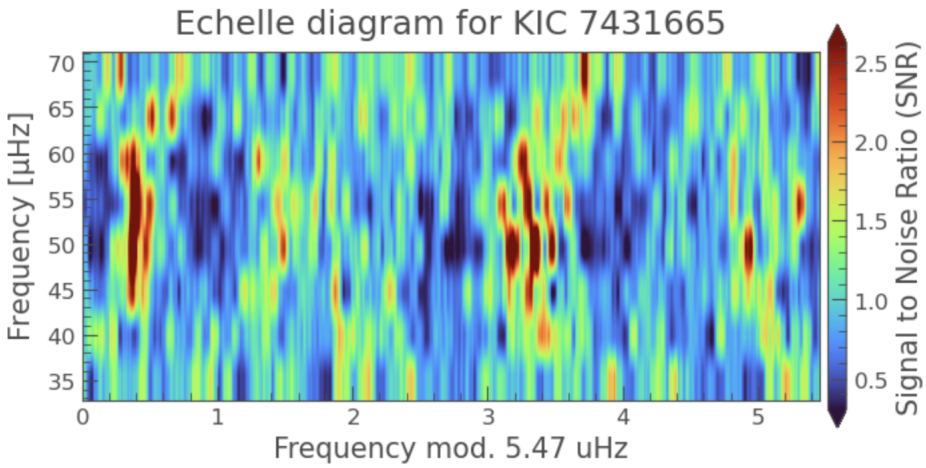

Figure 4. The Échelle diagram illustrates the oscillation modes for KIC7431665. The modes correspond to the vertical ridges with modes l=1, 2, 0 from left to right.

The strength of the vertical ridges for the frequency mod 5.47 μHz verifies that we can confidently perform calculations dependent on $\Delta\nu$, such as the scaling relations for stellar parameters. **Any other frequency spacing would produce an Échelle diagram with ambiguous or nonexistent ridges.**

4. DISCUSSION

The seismic analysis of KIC7431665 **updates the fundamental parameters in literature** by refining the results of pipeline projects that generalize the methodology to larger groups of stars. **This study also extends the asteroseismic analysis to the most recent *Kepler* data that covers 18 quarters of observations.** *Table 2* contains the stellar parameters from this study with a comparison to values from the literature of larger studies. For the comparison to the study by Beck et al. (2014) described in *Section 1*, we find percent differences of 1.24% and 0.16% for ν_{max} and $\Delta\nu$, respectively. **This study applied algorithms to 18 pulsating read giants following the methods of Kallinger et al. (2010) to estimate fundamental parameters. We also compare the results**

to the study conducted by Yu et al. (2018) which characterized the solar-like oscillations of 16,094 red giants. For the comparison to Yu et al. (2018), we find percent differences of 0.92% and 0.18% for ν_{max} and $\Delta\nu$, respectively.

Table 2. The results of this study for KIC7431665 compared to the results of previous pipeline studies. Reference 1: Beck et al. (2014); Reference 2: Yu et al. (2018).

	This work	Beck et al. (2014)	Yu et al. (2018)	**Percent Difference Beck et al. (2014)**	**Percent difference Yu et al. (2018)**
ν_{max} (μHz)	54.5 ± 0.4	54.0 ± 0.7	53.83 ± 1.04	0.92	1.24
$\Delta\nu$ (μHz)	5.47 ± 0.01	5.46 ± 0.02	5.461 ± 0.022	0.18	0.16
Radius ($R_\odot$)	9.58 ± 0.08	9.4 ± 0.1	9.49 ± 0.2	1.90	0.94
Mass ($M_\odot$)	1.43 ± 0.03	1.39 ± 0.05	1.14 ± 0.01	3.55	22.6
Luminosity ($L_\odot$)	36.2 ± 0.59	35 ± 2	35.5 ± 0.6	3.37	1.95
Log(g) (dex)	2.63 ± 0.001	2.62	2.639 ± 0.010	0.38	0.34

In addition to updating the stellar parameters from literature, this study constructs an Échelle diagram to begin a more detailed seismic analysis compared to the previous pipeline studies. The Échelle diagram reveals the presence of oscillation modes l=1, 2, and 0. **The strength of the oscillation modes present in the Échelle diagram serves as an independent method of finding the large separation frequency. The diagram also provides a preliminary understanding of the internal mechanisms of the star by illustrating evidence of both radial and dipole pulsations contributing to the solar-like oscillations.** The mix of radial and non-radial modes confirms the expected behavior of the star, but photometric observations do not capture all higher modes of oscillation within the star. A future study should obtain spectroscopic observations of KIC7431665 to detect higher non-radial modes of oscillation.

The fundamental parameters provide an important first step in stellar modeling. A future study of KIC7431665 should conduct a binary analysis to investigate the nature of the flux variations in the observed light curve. An **effective** binary analysis would separate the stellar pulsations from the binary features of the star. The residual pulsation frequencies would then indicate the presence of different types of stellar pulsations. We expect to find tidal pulsations due to the strong tidal forces at periastron, but other studies of heartbeat binaries reveal more interesting causes of pulsations, such as delta Scuti and gamma Doradus (Manuel & Hambleton 2018). A binary analysis of KIC7431665 would also confirm the stellar parameters presented in this study.

5. CONCLUSIONS

The asteroseismic study analyses the solar-like oscillations of KIC7431665 to reveal its stellar parameters. The *Kepler Input Catalog* provides detections from the *Kepler* mission for the target. A power spectrum generated from the light curve of the *Kepler* observations depicts clear power excess in the region of the mode envelope. The even spacing between the drops in flux indicates the oscillation modes present for the star. We apply a 2D-autocorrelation function to the region of excess power to determine the frequency of maximum power and the frequency difference between modes of the same radial order. We find ν_{max} = 54.5 ± 0.4 μHz and $\Delta\nu$ = 5.47 ± 0.01 μHz for KIC7431665. Applying scaling relations to the ν_{max} and $\Delta\nu$ for KIC7431665 yields the following stellar parameters: R = 9.58 ± 0.08 $R_\odot$, M = 1.43 ± 0.03 $M_\odot$, L = 36.2 ± 0.59 $L_\odot$, and log(g) = 2.63 ± 0.001 dex. The uncertainty ranges result **from applying error propagation to the standard errors from the bootstrapping resampling process.**

An Échelle diagram for KIC7431665 depicts the oscillation modes present in the photometric observations. We find modes of radial order l=1, 2, and 0. The strong vertical ridges formed by applying frequency mod 5.47 μHz provide a further verification of the parameters obtained from this study. As a result of this detailed asteroseismic analysis, we can confidently apply the stellar parameters for KIC7431665 to future stellar models and binary studies.

ACKNOWLEDGEMENTS

Thank you to Dr. Andrej Prša who assisted in the research process. A special thank you to Dr. Kelly Hambleton who offered expertise in the field of asteroseismology. We acknowledge the team that created LIGHTKURVE, the funding

for the *Kepler* Mission provided by NASA's Science Mission Directorate, and the *Kepler* team for making the data acquisition and analysis possible. Additionally, we would like to thank Michael C. Davis, Anthony J. LaBarca, Conor M. Larsen, and Kevin B. Moposita for supporting remarks and suggestions throughout the study. Thank you to the anonymous reviewers who provided scientific insight.

REFERENCES

Beck, P. G., Hambleton, K., Vos, J., et al. 2014, A&A, 564, A36, doi: 10.1051/0004-6361/201322477

Bedding , T. R., & Kjeldsen, H. 2010, Communications in Asteroseismology, 161, 3, doi: 10.1553/cia161s3

Bedding, T. R., & Kjeldsen, H. 2003, PASA, 20, 203, doi: 10.1071/AS03025

Bedding, T. R., Mosser, B., Huber, D., et al. 2011, Nature, 471, 608, doi: 10.1038/nature09935

Borucki, W. J., Koch, D., Basri, G., et al. 2010, Science, 327, 977, doi: 10.1126/science.1185402

Brown, A. G. A., Vallenari, A., Prusti, T., et al. 2021, Astronomy & Astrophysics, 650, doi: 10.1051/0004-6361/202039657e

Brown, T. M., Latham, D. W., Everett, M. E., & Esquerdo, G. A. 2011, AJ, 142, 112, doi: 10.1088/0004-6256/142/4/112

Carrier, F., & Eggenberger, P. 2006, AA, 450, doi: 10.1051/0004-6361:20054492

Cherinka, B., Andrews, B. H., Sánchez-Gallego, J., et al. 2019, The Astronomical Journal, 158, 74, doi: 10.3847/1538-3881/ab2634

De Moura, B. L., Beck, P. G., Di Mauro, M. P., et al. 2020, ApJ, 894, 67, doi: 10.3847/1538-4357/ab80c8

Efron, B. 1979, The Annals of Statistics, 7, 1. http://www.jstor.org/stable/2958830

Frasca, A., Molenda-Żakowicz, J., De Cat, P., et al. 2016, A&A, 594, A39, doi: 10.1051/0004-6361/201628337

Gilliland, R. L., Jenkins, J. M., Borucki, W. J., et al. 2010, ApJL, 713, L160, doi: 10.1088/2041-8205/713/2/L160

Guzik, J. A., Houdek, G., Chaplin, W. J., et al. 2016, ApJ, 831, 17, doi: 10.3847/0004-637X/831/1/17

Hon, M., Bellinger, E. P., Hekker, S., Stello, D., & Kuszlewicz, J. S. 2020, MNRAS, 499, 2445, doi: 10.1093/mnras/staa2853

Huber, D., Ireland, M. J., Bedding, T. R., & et al. 2012, ApJ, 760, doi: 10.1088/0004-637X/760/1/32

Huber, D., Bedding, T. R., Stello, D., et al. 2011, ApJ, 743, 143, doi: 10.1088/0004-637X/743/2/143

Kallinger, T., Mosser, B., Hekker, S., et al. 2010, A&A, 522, A1, doi: 10.1051/0004-6361/201015263

Kumar, P., Ao, C. O., & Quataert, E. J. 1995, ApJ, 449, 294, doi: 10.1086/176055

LeBlanc, F. 2010, An Introduction to Stellar Astrophysics

Lightkurve Collaboration, Cardoso, J. V. d. M., Hedges, C., et al. 2018, Lightkurve: Kepler and TESS time series analysis in Python, Astrophysics Source Code Library. http://ascl.net/1812.013

Lomb, N. R. 1976, Ap&SS, 39, 447, doi: 10.1007/BF00648343

Manuel, J., & Hambleton, K. 2018, in American Astronomical Society Meeting Abstracts, Vol. 231, American Astronomical Society Meeting Abstracts #231, 146.01

Mosser, B., & Appourchaux, T. 2009, A&A, 508, 877, doi: 10.1051/0004-6361/200912944

Prša, A., Harmanec, P., Torres, G., et al. 2016, AJ, 152, 41, doi: 10.3847/0004-6256/152/2/41

Scargle, J. D. 1982, ApJ, 263, 835, doi: 10.1086/160554

Seilmayer, M., Garcia Gonzalez, F., & Wondrak, T. 2020, arXiv e-prints, arXiv:2001.10200. https://arxiv.org/abs/2001.10200

Themeßl, N., Hekker, S., Southworth, J., et al. 2018, MNRAS, 478, 4669, doi: 10.1093/mnras/sty1113

Viani, L. S., Basu, S., Corsaro, E., Ball, W. H., & Chaplin, W. J. 2019, ApJ, 879, 33, doi: 10.3847/1538-4357/ab232e

Welsh, W. F., Orosz, J. A., Aerts, C., et al. 2011, ApJS, 197, 4, doi: 10.1088/0067-0049/197/1/4

Yu, J., Huber, D., Bedding, T. R., et al. 2018, VizieR Online Data Catalog, J/ApJS/236/42

Zhang, X., Li, Y., Wu, T., & Su, J. 2020, MNRAS, 494, 511, doi: 10.1093/mnras/staa667